Brazilian Journal of Physics (2022) 52: 51
https://doi.org/10.1007/s13538-022-01060-4

GENERAL AND APPLIED PHYSICS

# Application of Electron Spin Resonance Spectroscopy in Bone Regeneration Studies

Gisele Janaina Blasioli[1] · Lucas Henrique Pereira Silva[2,3] · Leandro Andrade Holgado[1] · Tatiana Peixoto Telles de Sousa[1] · Sergio Augusto Catanzaro Guimarães[4] · Oswaldo Baffa[5] · Angela Kinoshita[2]

Received: 23 November 2021 / Accepted: 17 January 2022 / Published online: 2 February 2022


**Abstract**
Electron spin resonance (ESR) is a spectroscopic technique that detects unpaired electrons, such as the ones present in free radicals. When a calcified tissue is irradiated, free radicals are generated, like the $CO_2^-$. This paper presents a preliminary study on the application of this spectroscopic technique for monitoring bone mineralization processes during the bone repair in animal model, induced by polyurethane in two forms, as an occlusive membrane and as a bone grafting. In the first experiment, the ESR results and microscopic analysis demonstrate centripetal bone growth and advanced stage of bone regeneration in the treated group. In the second experiment, the ESR spectrum of collected bone pieces presents the superposition of the spectrum of the biomaterial and the radical $CO_2^-$. The separation of the components was made using spectral simulation, and the percentage of mature bone tissue in the defect region was determined through the comparison with the spectrum of the native bone. In both experiments, ESR provided results consistent with microscopic analysis, demonstrating the feasibility of the technique for monitoring bone regeneration.

**Keywords** Electron spin resonance · Bone regeneration · Biomaterial · Polyurethane

## 1 Introduction

Bone plays important mechanical functions in the human body, presents a strong regeneration potential, being able to repair fractures or local defects with structural organization highly similar to the original. Skeletal tissue is composed of cells (the main are osteoblasts, osteoclasts, and osteocites) and an extracellular matrix (ECM), constituted mainly by type-I collagen. This component assigns flexibility to bones. Among the collagen fibers, there are apatite crystals, especially hydroxyapatite, HAp ($Ca_{10}(PO_4)_6(OH)_2$) that attribute rigidity to bones [1].

When the bone is injured, physiological processes are sequentially triggered for the correct repair of the damaged area, and the last step is the mineralization of the ECM. During bone repair and neoformation, important structures associated with bone tissue such as the periosteum and endosteum respond with intense proliferation. The formation of osteogenic connective tissue begins; an immature or primary bone tissue is produced where small islands of mineralization are present. This process evolves, with the confluence of these mineralized islands, leading to a greater organization of collagen fibers in lamellae, as well as an intensification in the mineralization process. Gradually, the primary bone tissue is replaced by a more organized bone tissue. This lamellar organization is concentric, with vascular channels, forming the Havers Systems. These mineralization characteristics, associated with the presence of the Havers systems, denote bone maturity, named as secondary or lamellar bone. Thus, the mineralization of skeletal tissue is an indicator of tissue maturity in bone repair/regeneration processes [2].

✉ Angela Kinoshita
angelamitie@gmail.com; angela@unoeste.br

1 Centro Universitário Sagrado Coração, Unisagrado, Bauru, 17.011-160, São Paulo, Brazil

2 Universidade Do Oeste Paulista, UNOESTE, Presidente Prudente, 19067-175 São Paulo, Brazil

3 Instituto Federal de São Paulo, Presidente Epitácio, SP, São Paulo, Brazil

4 FOB-Faculdade de Odontologia de Bauru, Universidade de São Paulo, Bauru, 17012-90 São Paulo, Brazil

5 Departamento de Física, FFCLRP, Universidade São Paulo, Ribeirão Preto, 14049-900 São Paulo, Brazil

Clinically, bone mineral density can be obtained by bone densitometry or dual energy X-ray absorptiometry (DXA), a method presented in the 60 s by Cameron and Sorenson [3], which is based on the measurement of the attenuation suffered by two monochromatic beams of X-rays of different energies. Currently, this is the standard method used for diagnosing osteoporosis, among other situations where bone mineral density should be assessed. Bone mineral density can also be inferred using other radiographic methods such as radiography and computed tomography [4]. In studies using animal models, as is the case in this work, the quantification of histological images of slices of tissue is the most used method. However, new methods for analysis are always welcome, in order to improve the elucidation of the processes involved.

Electron spin resonance (ESR) is a spectroscopic technique that detects systems with unpaired electrons, especially free radicals. Some of them are not "naturally" present in calcified tissues, but can be created through the interaction with ionizing radiation (X-rays, γ-rays, or UV). Radicals generated in the organic part of bones are unstable, but the radicals generated in the mineral part (HAp) are stable and can be detected and quantified by ESR. The main radical generated by ionizing radiation in mineralized tissues is $CO_2^-$ and is due to the presence of carbonate impurities ($CO_3^{2-}$) [5, 6].

The use of ESR in hard tissues is traditionally done in ionizing radiation dosimetry and archaeological/paleontological dating. They are based on the detection of $CO_2^-$ radicals, created by ionizing radiation on the mineral matrix of these tissues. The amount of these radicals is proportional to the radiation dose, consisting of a dosimetric method capable of using tissues of the human body as a dosimeter, very useful in cases of accidental exposure to ionizing radiation. This pioneering idea was presented by Prof. Sérgio Mascarenhas in the 70 s, when he studied bones of Hiroshima bomb victims through investigations done at the University of Hiroshima. Preliminary results of the "magnetic memory" present in the irradiated bones were presented in 1973 [7] and, years later, advances in instrumentation and technique allowed new evaluation and publication of complete results [8]. Currently, ESR dosimetry using dental enamel is a well-established method to retrospective dosimetry in accidental cases of exposition, with technical report published by International Atomic Energy Agency (IAEA-TECDOC-1331) [9]. Dosimetry using bones was also used to assess the dose of radiation deposited by radiopharmaceuticals, intended for palliative treatment of pain caused by bone metastases, that is, situation in which there is no way to install dosimeters to perform traditional dosimetry [10]. Other calcified tissues as shells have also been proposed for radiation dosimetry [11, 12].

In ESR dating, the radiation dose is converted into age from the calculation of the annual dose rate of radiation of the environment where the material was collected [13]. The first ESR dating study in Brazil was performed by our group using bones and shells [14]. Subsequently, the dating of fossil materials (shell, tooth, calcite) collected in different locations in Brazil was carried out, contributing, for example, to the reconstruction of the events that led to the extinction of certain species [15, 16], indicating the presence of humans in the pre-history in Brazil [17–20] and for studies on geological formation of the coastal line of the southern of Brazil [21, 22].

The use of ESR to study the mineralization of the hard tissue has the same principles of the radiation dosimetry. Considering a homogeneous sample (bone, dentin, or enamel), the ESR signal intensity will be a function of the radiation dose. Therefore, in a non-homogeneous tissue sample irradiated with the same dose, the ESR signal intensity in each piece of tissue will be proportional to the mineralization, that is, the intensity of the spectrum is proportional to the amount of HAp present.

This work aims to evaluate whether electron spin resonance can be used to determine the mineralization in the bone repair process. Two models were used, in the first, surgically induced defects were treated with guided bone regeneration (GBR) [16] using an occlusive membrane of polyurethane. In the second, the defects were treated with polyurethane in the form of granules that acted as graft material. The information of mineralization could be useful in the future, as an indicator of the quality of regenerated bone.

## 2 Material and Methods

### 2.1 Animals and Surgical Procedure

The present study was approved (protocol 26/07), prior to the beginning of the experiments, by the Ethical Committee from the Universidade Sagrado Coração – USC, Bauru, São Paulo State, Brazil. A total of 27 male New Zealand adult rabbits, weighting an average of 4.0 kg were used. The rabbit is one of the most frequently used animal models for medical research, comprising approximately 35% of musculoskeletal system research studies [23, 24]. Rabbit has a similar bone metabolism to humans, making it the first choice in evaluating bone graft materials [25]. These animals were housed in temperature-controlled rooms and received water and food *ad libitum*. A full thickness bone defect of 5 × 15 mm was surgically created in the skull (Fig. 1). Preoperatively, deep sedation was intramuscularly induced in animals with xylazine chlorhydrate (5 mg/kg, Bayer, Brazil) and ketamine (35 mg/kg Vetbrands, Brazil). The dorsal part of the cranium was shaved and aseptically prepared for surgery. A

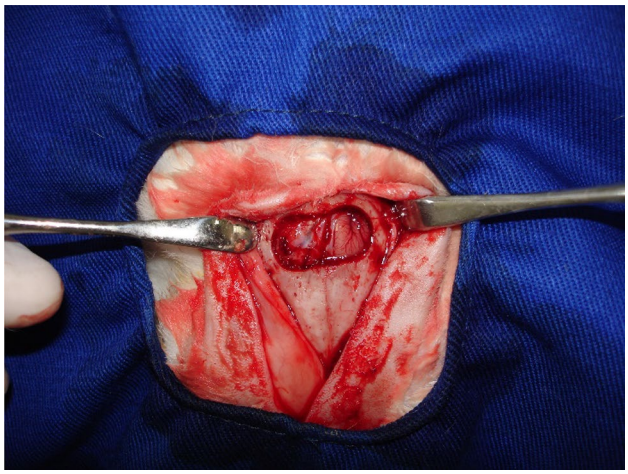

**Fig. 1** Bone defect (5 × 15 mm) surgically created in rabbit calvaria

linear incision of 5 cm long was made on the skin at the median sagittal line. The musculature and the periosteum were reflected, exposing the parietal bone, and a full thickness cranial defect 15 mm × 5 mm was carefully created, by means of a trephine bur operating with low rotation under irrigation with sterile physiological solution (0.9% NaCl). Cortical and spongious bones were totally removed, and dura mater was exposed (Fig. 1).

Eighteen defects were treated by GBR and nine by grafting as described in the following section.

#### 2.1.1 Guided Bone Regeneration

Two membranes of polyurethane were adapted, one in contact with the dura mater and the other, in the surface defect (Fig. 2A, B). In the control group ($N = 9$), the defect remained filled with clot. The soft tissues and skin incisions were closed with 4–0 silk interrupted sutures. After 30, 60, and 120 days post-surgery, three animals from each group were euthanized, in an isolated room with no sensory access to other animals, and specimens containing bone defect was collected.

#### 2.1.2 Bone Grafting

In this experiment, the defect (Fig. 1) was treated with 50 mg of polyurethane pellets in association with clot. The soft tissues and skin incisions were closed with 4–0 silk interrupted sutures. After 30, 60, and 120 days post-surgery, three animals were euthanized, and specimens containing bone defect were collected to microscopic an ESR analysis.

### 2.2 Optical Microscopic Analysis

The bone samples were kept 92 h in phosphate buffered formalin (10%) and divided in 2 parts. One of them was used for ESR experiments and the other to microscopic analysis.

The samples for microscopy were decalcified using Morse Method and processed for evaluation (6-μm thick sections and Masson Trichromic stain). The specimens were analyzed with an optical microscope Nikon H550L.

### 2.3 Electron Spin Resonance Experiments

#### 2.3.1 Guided Bone Regeneration

The samples selected for ESR experiment were cleaned with water and alcohol and dried in a vacuum for 15 days. Then, they were irradiated with 3 kGy of γ-rays through IPEN (Instituto de Pesquisas Energéticas e Nucleares) Gammacell source at a dose rate of 634 Gy/h, using a buildup layer to obtain the electronic equilibrium. A fraction of approximately 50 mg of the native bone (NB), the bone at the edge of the defect (E) region, and at the center of the defect (C) of the samples were extracted and weighed. The ESR spectrum was acquired in the JEOL FA200 X-Band spectrometer, set with central field 338 mT, modulation amplitude 0.1 mT, modulation frequency 100 kHz, scan width 10 mT,

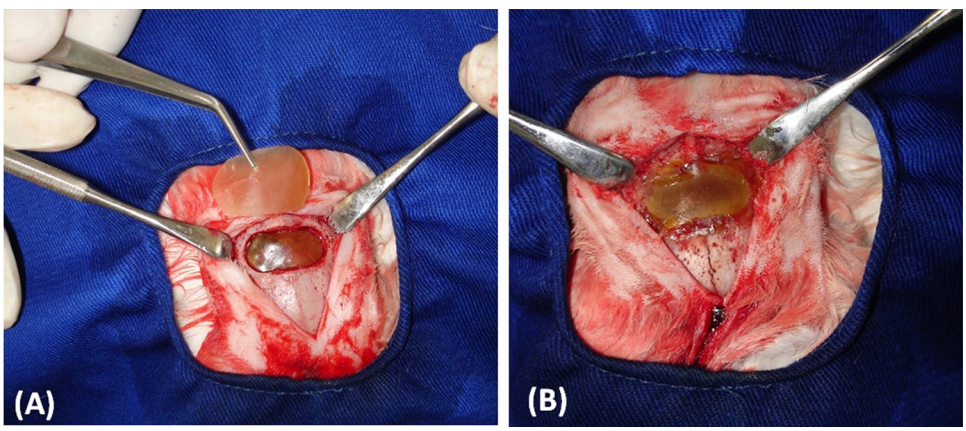


**Fig. 2** Guided bone regeneration (GBR) treatment of defects. (**A**) Photograph showing the membrane positioned over the dura mater and the second, to be implanted. (**B**) GBR treatment finished with the second membrane positioned over the defect. The size of defect is 5 × 15 mm

microwave power 2 mW. The signal intensity normalized by mass of the 3 regions were determined: $I_{NB}$, $I_E$, and $I_C$. The mineralization degree in each region was calculated by the ratios: $I_E/I_{NB}$, and $I_C/I_{NB}$.

#### 2.3.2 Bone Grafting

The samples selected for ESR experiment were cleaned with water and alcohol and dried in a vacuum for 15 days. The material present in the defect region was extracted and weighed. As the polyurethane pellets are irradiated for sterilization (by the manufacturer with a dose of 25 kGy of gamma radiation), it presents an ESR signal. Thus, by recording the ESR spectrum of the material of a known quantity, there is a relationship between ESR intensity and grafted material mass. So, firstly the spectrum of the sample from the defect region was acquired and corresponds to the signal of the polyurethane, and its mass was determined, using the previously explained relationship. The ESR spectrum was acquired in the JEOL FA200 X-Band spectrometer, set with the same parameters of the GBR experiment. The polyurethane mass value was subtracted from the mass of the sample collected, and thus the value of the mass of the tissues contained in each one is obtained. After that, these samples were irradiated with 3 kGy, as the GBR experiment, and also approximately 50 mg of the native bone (NB). The spectra of the native bone and the material present in the defect (D) region were acquired for further signal processing. The software Simfonia (Bruker) was employed to separate the 2 components of the spectrum of the defect (D) region to determine the signal intensity of the $CO_2^-$radical which was divided by the mass of the tissues of the defect region, corresponding to the $I_D$. The mineralization degree of the region was calculated by the ratio: $I_D/I_{NB}$.

## 3 Results

### 3.1 Guided Bone Regeneration

Figure 3 shows the photomicrographs of samples of treated A and control B groups of the bone defect region, in the period of 30 days post-surgery, in which we can more easily notice the difference produced by the treatment. In both groups, there was no presence of cartilage, showing the direct osteonal ossification. In the treated-group image (Fig. 3A), bone trabeculae in linear disposition can be seen (bt) extending on the external and internal surface of the defect, which are arranged in two bands representing the external and internal tables of the cranial bone. Bone bridges made up of immature bone tissue and bone tissue undergoing remodeling are seen joining the external and internal bone tables. Some areas show an aspect of medullary structure in early formation (bm).

In the control-group image (Fig. 3B), immature bone tissue is observed close to the edges of defect, immature bone tissue (ib) in the right end is observed in the form of trabecular clusters, in the left end there is reticular immature bone tissue projecting to the center of the defect. Osteogenic connective tissue (ct) filling the central part of the defect can be seen.

Figure 4 shows the ESR spectra of the native, the edge of the defect, and the center of the defect from a sample of the treated group. The ESR signal intensity: $I_{NB}$, $I_E$, and $I_C$

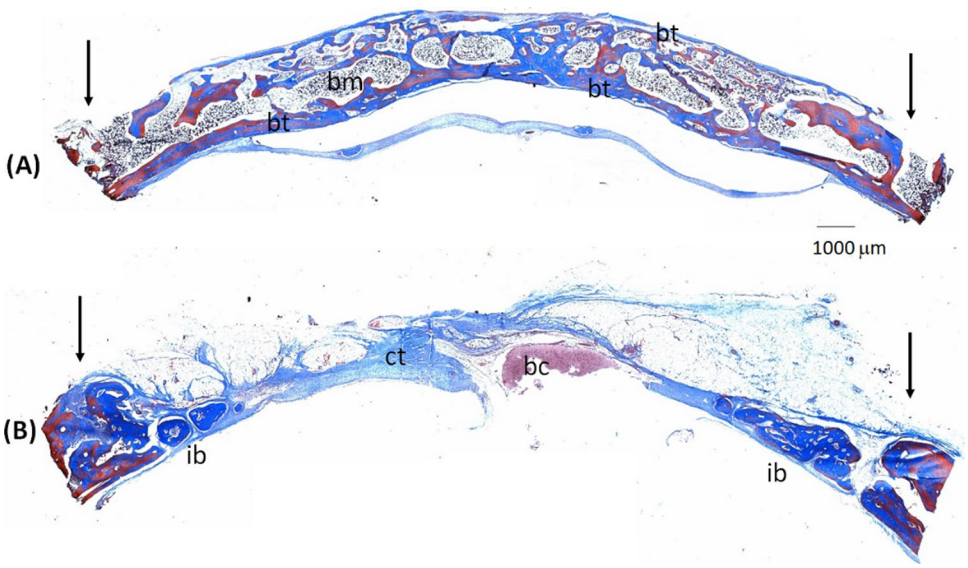


**Fig. 3** Photomicrographs of the histological sections of bone defect (Masson's Trichrome stain, 2×) 30 days after surgery, showing the limits of region of defect (black arrow). (**A**) GBR-treated group, showing an advanced stage of regeneration in comparison with control group. bt: bone trabeculae and bm: bone marrow (in formation). (**B**) Control group, showing the defect filled with connective tissue (ct) and some immature bone (ib) at edges of the defect. bc: blood clot

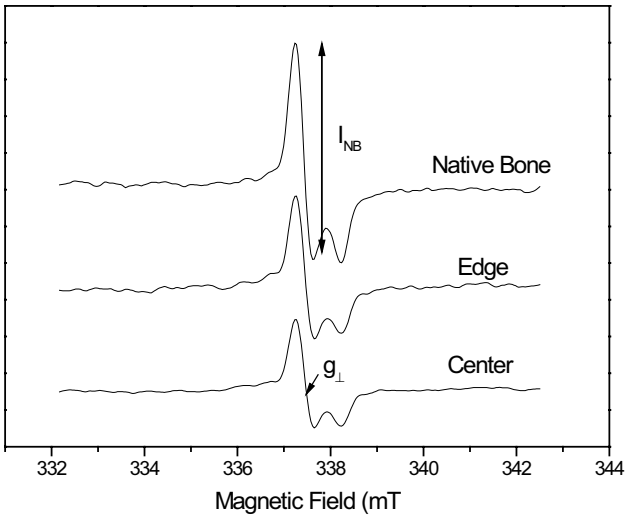


**Fig. 4** ESR spectra of native bone (NB), the edge (E), and the center (C) of defect, normalized by mass of 60-day period of the treated group

were measured at $g_{\perp}$, as indicated. In this spectra, $I_E/I_{NB}$ is 70.9% and $I_C/I_{NB}$ is 52.0%.

Figure 5 shows the mineralization degree obtained by ESR according to the groups, region of the bone, and periods post-surgery. The results indicate a centripetal direction of bone regeneration; the bone at the edge of defect is more mineralized than of the center, that is in agreement with the microscopic images. The results of 30-day samples also show that the use of membranes accelerated the bone repair in the center of the defect. There are statistically significant differences between the means ($p < 0.05$ *t*-Student test) in the comparison of the results of groups.

## 3.2 Bone Grafting

Figure 6 shows photomicrographs of the region of defect grafted with polyurethane. The images show the progress of bone regeneration by osteoconduction. The direct ossification without the presence of cartilage and absence of foreign body inflammatory reaction were observed in all periods studied. The last feature is related to the biocompatibility of the biomaterial.

The photomicrograph of the period of 30 days (Fig. 6A) shows newly formed bone (nfb) tissue firmly adhered to the surface of the polyurethane particle (p) through a thin layer of the bone matrix fixed to the contact surface. As already mentioned, the graft material stimulates bone formation through osteoconduction. In the 120-day photomicrograph (Fig. 6B), the newly formed bone tissue coating the biomaterial presents more mature with the formation of mineralized bone matrix on the surfaces of osteointegrated particles. In this interface, lamellar bone (lb) is present.

The ESR spectrum of the defect region where the polyurethane was implanted was registered before and after irradiation. Initially, the spectrum corresponds to the signal of the biomaterial. A fraction of irradiated native bone tissue was also recorded. Figure 7 demonstrates the spectra of the samples collected 30 and 120 days post-surgery.

The spectrum of $CO_2^-$ was simulated with the software Simfonia (Bruker) and subtracted from the composed spectrum (bone and polyurethane). The result fits well with the

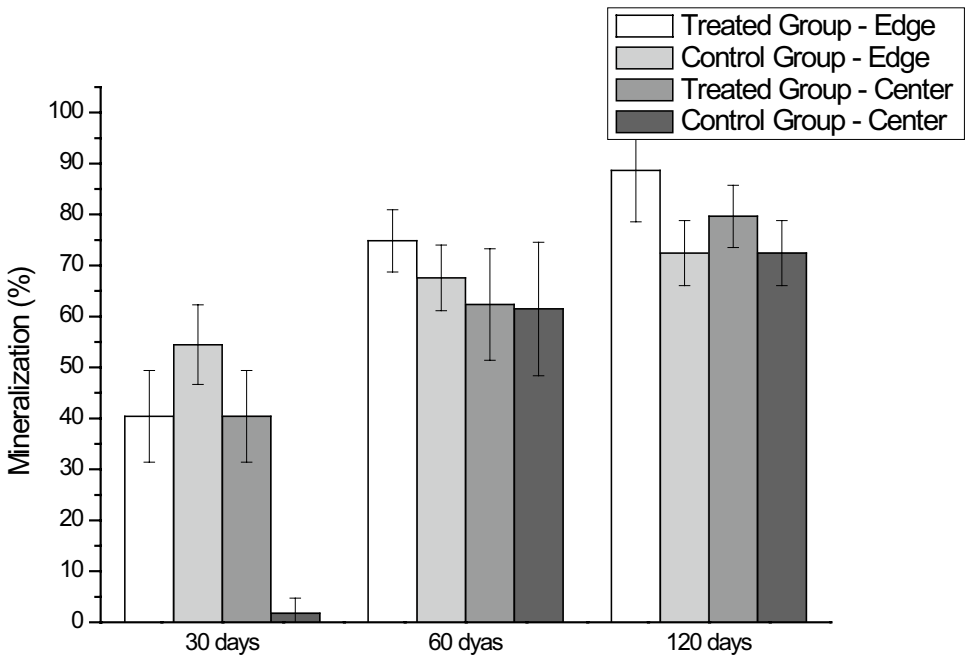


**Fig. 5** Mean and standard deviation of the ratios $I_E/I_{NB}$, and $I_C/I_{NB}$ for the groups, according to the periods of 30, 60, and 120 days post-surgery

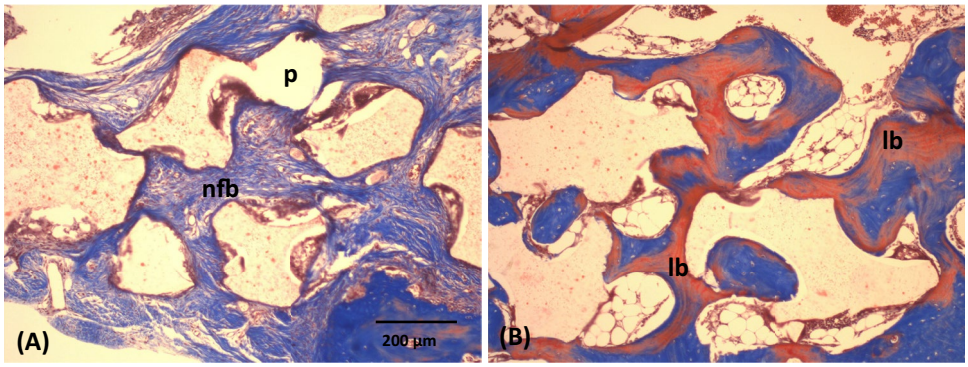


**Fig. 6** Photomicrographs of the region of defect grafted with polyurethane pellets (**A**) 30 day, (**B**) 120 days post-surgery (bar = 200 µm). p = Polyurethane, nfb: newly formed bone, lb: lamellar bone

initial spectrum of polyurethane. The $CO_2^-$ radical intensity (from mineralized part of bone) is higher in the spectrum at 120 days, which is in agreement with the microscopic results. The mean values obtained for the mineralization degree are $6.3 \pm 0.7\%$; $25.3 \pm 5.2\%$, and $26.4 \pm 5.1\%$ for the periods of 30, 60, and 120 days.

The absence of foreign body inflammatory reaction due to the implant of polyurethane in both experiments is associated to the biocompatibility of this biomaterial. It was already related by other authors, which used this biomaterial in tissue reconstruction [26, 27].

## 4 Discussion

The reconstruction of defects with great magnitude due to traumas, tumors, infections, and abnormalities in development, is highly difficult, mainly due to the growth of connective tissue at the injury site. This tissue is an obstacle to bone regeneration; it may disturb or totally prevent osteogenesis. To try to prevent the occupation of the defect site with connective tissue, several procedures were used as grafts, implants, and also the technique of guided bone regeneration (GBR), which has been proved as an effective method to stimulate regeneration in bone defects for more than a decade [28, 29]. The use of occlusive membranes is effective in guided bone regeneration when used as barriers, preventing invasion of cells and non-osteogenic tissues in the area of the defect. This allows the local occupation by osteogenic cells that will guide bone regeneration [30].

The use of grafts favors the repair process by filling the bone defect, leading to bone neoformation through the osteoconduction process. In this process, bone neoformation is conducted by materials with a specialized structure, which fill the bone defect and act as a scaffold for bone cell penetration and growth in its surroundings. The implanted

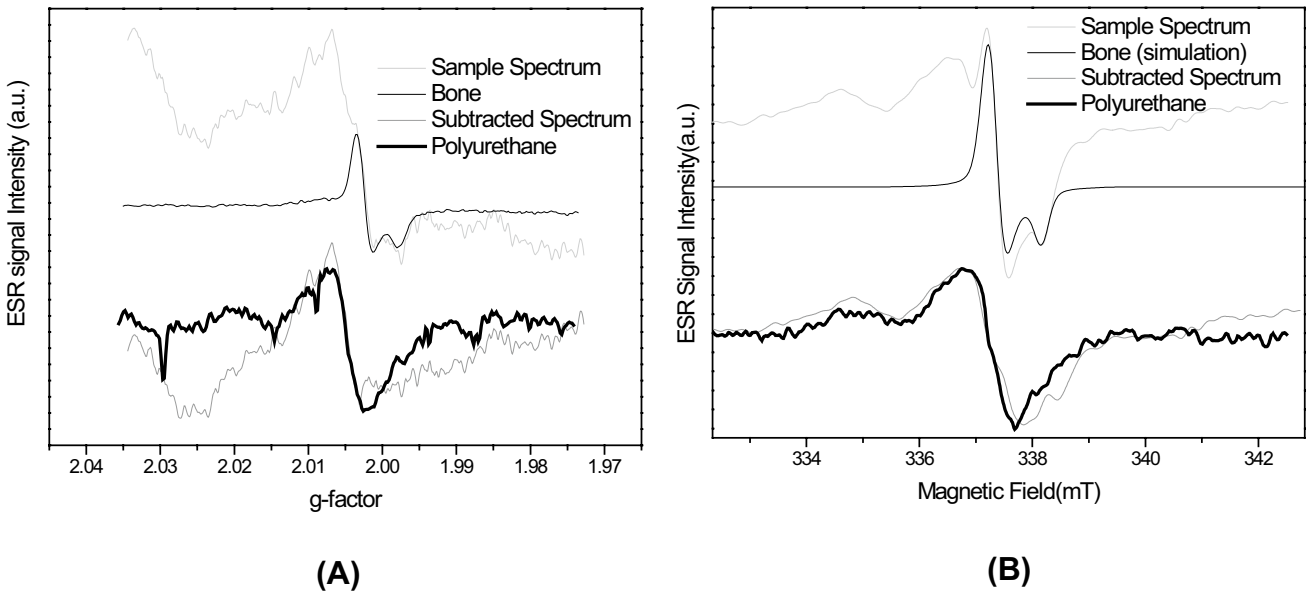


**Fig. 7** ESR spectra of sample from defect region before (bold black line) and after irradiation (light gray line), from the native bone (black line) and subtracted spectrum (gray line). (**A**) 30 days, (**B**) 120 days

material serves as an anchor for the growth of capillaries, perivascular tissue, and undifferentiated osteoprogenitor cells originated in the surgical bone bed, and also prevents non-osteogenic tissues from invading the site to be repaired. Bone grafts are widely used in medicine, plastic and orthopedic surgery and in dentistry, in large maxillomandibular reconstructions, and small increases in bone height, enabling the placement of bone implants [31]. Specifically, polyurethane is a well-studied material, with proven biocompatibility and good performance [32–35].

Some studies of bone tissue mineralization by specialized physical–chemical techniques have already been carried out by Raman spectra, Fourier transform infrared spectroscopy (FTIR), and X-ray diffraction (DRX) [1]. Specifically using ESR, the study of Baffa et al. [36] demonstrated, preliminarily, that hydroxyapatite crystals are organized in the same direction as the main axis of bone growth.

In the present work, the histological images of the region of the defect in both experiments demonstrate the results predicted by the treatments, with advances in the bone regeneration process in relation to the control group (Fig. 3) and growth and maturation of bone tissue around the material (Fig. 6). The success of the bone repair process can be determined by the degree of bone mineralization produced. Thus, in this work, the results obtained by ESR in both models corroborate the observations in microscopic images, demonstrating a quantitative method for determining mineralization during the bone repair process.

## 5 Conclusions

The detection of radical induced by ionizing radiation in mineralized tissues by electron spin resonance allows the monitoring the dynamics of bone regeneration. As the mineralization is the last stage of bone healing, this could be used as an indicator of the quality of the regenerated bone.

**Acknowledgements** The authors are grateful to Professor Sergio Mascarenhas to whom we dedicate this article and who, through his pioneering work in the 1970s on physical aspects of hard tissues, such as bones and teeth, which resulted in several articles, theses and dissertations, drew attention to this area of interdisciplinary research.

**Funding** This work received funding from Fundação de Amparo à Pesquisa do Estado de São Paulo (FAPESP) Grants 03/09505–6, 07/06720–4 & 2013/07699–0, Conselho Nacional de Desenvolvimento Científico e Tecnológico (CNPq) Grants 304107/2019–0 and 309186/2020–0 and Coordenação de Aperfeiçoamento de Pessoal de Nível Superior (CAPES) código 001.

## Declarations

**Conflict of Interest** The authors declare that they have no conflict of interest with any organization regarding the material discussed in this manuscript. This work was partially supported by the research funding agencies as mentioned and it was conducted in accordance with ethical academic standards and also respecting ethical guidance for animal studies. The preliminary version of this work was presented at the 18th International Conference on Medical Physics (April 17-20, 2011 Porto Alegre - RS - Brazil) and an abstract was published.

## References

1. M. Murshed, Cold Spring Harb. Perspect. Med. **8**, 1 (2018)
2. L. J. Raggatt, N. C. Partridge, **285**, 25103 (2010)
3. J. R. Cameron, J. Sorenson, Science (80-. ). **142**, 230 (1963)
4. P.D. Miller, Bone **104**, 4 (2017)
5. P. Fattibene, F. Callens, Appl. Radiat. Isot. **68**, 2033 (2010)
6. F. Callens, R. Verbeeck, P. Matthys, L. Martens, E. Boesman, Calcif. Tissue Int. **41**, 124 (1987)
7. S. Mascarenhas, A. Hasegawa, K. Takeshita, Bull Am Phys Soc **18**, 579 (1973)
8. A. Kinoshita, O. Baffa, S. Mascarenhas, PLoS One **13**, e0192444 (2018)
9. IAEA, Use of Electron Paramagnetic Resonance Dosimetry with Tooth Enamel for Retrospective Dose Assessment (TECDOC Series, 2002). https://www-pub.iaea.org/MTCD/Publications/PDF/te_1331_web.pdf. Accessed 25 Jan 2022
10. A. Kinoshita, F. Braga, C.F.O. Graeff, O. Baffa, Appl. Radiat. Isot. **54**, 269 (2001)
11. M. Ikeya, J. Miyajima, S. Okajima, Jpn. J. Appl. Phys. **23**, L697 (1984)
12. C. Fainstein, Brazilian. J. Phys. **36**, 90 (2006)
13. M. Ikeya, *New applications of electron spin resonance: Dating, dosimetry and microscopy* (World Scientific, New Jersey, USA, 1993)
14. S. Mascarenhas, O.B. Filho, M. Ikeya, Am. J. Phys. Anthropol. **59**, 413 (1982)
15. L. dos S. Avilla, A. M. Graciano Figueiredo, A. Kinoshita, C. Bertoni-Machado, D. Mothé, L. Asevedo, O. Baffa, V. H. Dominato, Quat. Int. **305**, 85 (2013)
16. R. L. Azevedo, V. K. Asfora, D. S. Mützenberg, D. Cisneiros, H. L. Sullasi, A. M. Kinoshita, P. L. Guzzo, A. R. Skinner, O. Baffa, A.-M. Pessis, H. J. Khoury, Quat. Int. **556**, (2020)
17. A. Kinoshita, L. Figuty, O. Baffa, Brazilian. J. Phys. **36**, 93 (2006)
18. A. Kinoshita, H. L. Sullasi, V. K. Asfora, R. L. Azevedo, P. Guzzo, N. Guidon, A. G. F. Maria, H. Khoury, A.-M. Pessis, O. Baffa, An. Acad. Bras. Cienc. **88**, (2016)
19. A. Kinoshita, A. R. Skinner, N. Guidon, E. Ignacio, G. D. Felice, C. D. a Buco, S. Tatumi, M. Yee, A. M. G. Figueiredo, O. Baffa, J. Hum. Evol. **77C**, 187 (2014)
20. S. Watanabe, W. E. F. Ayta, H. Hamaguchi, N. Guidon, E. S. La Salvia, S. Maranca, O. Baffa Filho, J. Archaeol. Sci. **30**, 351 (2003)
21. R. P. Lopes, J. C. Pereira, A. Kinoshita, M. Mollemberg, F. Barbosa, O. Baffa, J. South Am. Earth Sci. **101**, 102605 (2020)
22. R. P. Lopes, J. C. Pereira, S. R. Dillenburg, S. H. Tatumi, M. Yee, A. M. G. Figueiredo, A. Kinoshita, O. Baffa, J. South Am. Earth Sci. **100**, 102566 (2020)
23. J. A. McGovern, M. Griffin, D. W. Hutmacher, Dis. Model. Mech. **11**, (2018)
24. R.I. Falacho, P.J. Palma, J.A. Marques, M.H. Figueiredo, F. Caramelo, I. Dias, C. Viegas, F. Guerra, Molecules **26**, 1339 (2021)
25. Y. Li, S.-K. Chen, L. Li, L. Qin, X.-L. Wang, Y.-X. Lai, J. Orthop. Transl. **3**, 95 (2015)

26. V.M.R. Barros, A.L. Rosa, M.M. Beloti, G. Chierice, J. Biomed. Mater. Res. Part A **67A**, 235 (2003)
27. O.C.M. Pereira-Júnior, S.C. Rahal, P. Iamaguti, S.L. Felisbino, P.T. Pavan, L.C. Vulcano, J. Biomater. Appl. **21**, 283 (2007)
28. P. Gentile, V. Chiono, C. Tonda-Turo, A.M. Ferreira, G. Ciardelli, Biotechnol. J. **6**, 1187 (2011)
29. C. Dahlin, E. Sandberg, P. Alberius, A. Linde, Int. J. Oral Maxillofac. Surg. **23**, 237 (1994)
30. D. D. Bosshardt, R. K. Schenk, in *20 Years Guid. Bone Regen. Implant Dent.*, ed. by D. Buser, 2nd ed. (Quintessence, Chicago, 2010), pp. 15–46
31. F.J. O'Brien, Mater. Today **14**, 88 (2011)
32. T. P. T. De Sousa, M. S. T. Da Costa, R. Guilherme, W. Orcini, L. de A. Holgado, E. M. Varize Silveira, O. Tavano, A. G. Magdalena, S. A. Catanzaro-Guimarães, A. Kinoshita, Polimeros **28**, 246 (2018)
33. G. C. Belmonte, S. A. Catanzaro-Guimarães, T. P. T. De Sousa, R. S. Carvalho, A. Kinoshita, G. O. Chierici, Polimeros **23**, (2013)
34. R. R. C. Da Costa, F. R. B. De Almeida, A. A. X. Da Silva, S. M. Domiciano, A. F. C. Vieira, Polimeros **29**, (2019)
35. I. Chakraborty, K. Chatterjee, Biomacromol **21**, 4639 (2020)
36. O. Baffa, J.R. Olivieri, S. Mascarenhas, O.R. Nascimento, Brazilian J. Med. Biol. Res. **16**, 396 (1983)